Aust. J. Phys., 1987, **40**, 47–60

A Photodetector for Measurement of Metastable H(2S) in Ion–Atom Collisions

D. G. Williams, A. R. Lee and E. C. Butcher

Department of Physics, La Trobe University,
Bundoora, Vic. 3083.

Abstract

The Stark effect is employed in the detection of fast metastable hydrogen in the energy range 4–24 keV. A consideration of the design of a detector is presented in the light of recent work describing the decay process.

1. Introduction

The method generally employed to detect the uncharged metastable component in a scattered hydrogen beam is to subject the beam to a sufficiently strong electric field to induce decay of the metastable state via the Stark effect. The resulting Lyman α photon flux is easily detected and corresponds to the metastable flux. This electric field quenching is simple to implement but an understanding of the processes involved in the conversion from the metastable state to the photon, and particularly the detection of the photon, has to be thorough if certain pitfalls are to be avoided in the design. This paper gives details of the considerations made in the design of a metastable particle detector employed to measure angular scattering of metastable hydrogen in the electron capture process:

$$H^+ + H_2 \rightarrow H(2S) + H_2^+ . \qquad (1)$$

Scattering experiments observing excited states, some employing metastable hydrogen detectors, have been reviewed by Thomas (1972) and Brouillard (1981) and are not repeated here. However, features of some of these designs are discussed. The main aim in the present paper is to describe the design of a detector sensitive enough to measure angular scattered flux and which has a detection efficiency almost constant with projectile energy. These requirements are complicated by several factors, namely, (i) the applied electric field is not spatially constant; (ii) the fraction of flux quenched per unit beam length depends on the magnitude of the electric field at that point; (iii) the radiation from the decayed metastable particle is anisotropic about the direction of the applied electric field, the amount of anisotropy being dependent on the field strength at that point; and (iv) the distribution of photons emitted along the beam path changes with particle speed, and the photon detector must cope with this variation. These factors will be considered in this paper.

0004-9506/87/010047$02.00

2. Preliminary Considerations

The theory describing the hydrogen atom when subjected to a time-independent electric field has been described in detail by Bethe and Salpeter (1957) and later verified experimentally for the 2S state by Sellin (1964). The electric field deforms the hydrogen atom so that the positive and negative charges no longer coincide and a dipole moment is produced. For quantum mechanical calculations the deformed state must now be described as a linear combination of the field-free S state and the P states. This contribution from the P states reveals that single photon emission is now possible and its rate depends on the amount of deformation of the atom (and therefore on the magnitude of the applied field); the decay to the ground state (2S–2P–1S) is now possible with a resulting 121·6 nm photon. The lifetime for the process has been derived by Bethe and Salpeter (1957) for electric fields less than 1000 V cm^{-1}, i.e.

$$t(2S) = t(2P)\left(1 + \frac{F^2}{\{1-(1+F^2)^{\frac{1}{2}}\}^2}\right), \tag{2}$$

where

$$F = \tfrac{1}{475} E, \tag{3}$$

$t(2S)$ is the lifetime of the 2S state in the electric field, $t(2P)$ is the lifetime of the field-free 2P state, and E is the magnitude of the electric field (V cm^{-1}).

The lifetimes of the hyperfine S states are different but have negligible effect on the fraction of the flux that is quenched (Drake and Grimley 1975; Drake *et al.* 1975). For a constant electric field the fraction of the total metastable flux which has decayed at time T after entering the field is

$$f = 1 - \exp\{-T/t(2S)\}. \tag{4}$$

The quenching effect may be used to separate the metastable state from the other excited states. The particle flux is subjected to an electric field (hereafter referred to as the quenching cell), within the view of a photon detector, at a position where the beam has travelled a distance from the formation point of the excited states such that the time required for the travel between these points is much greater than the lifetime of the short lived excited states. These short lived excited states will have decayed to a negligible proportion (Homma *et al.* 1982) of the total flux but the metastable component would have hardly decayed at all. However, the separation is not complete due to the possibility of hydrogen atoms in higher excited states cascading to the metastable state. The resulting change in the flux of metastable particles may not be negligible and has to be considered.

There are various sources of gain in the number of metastable particles registered by the detector:

(i) Electron capture from the residual gas may occur in the region between the target and the quenching cell.

(ii) Electron capture from the residual gas to a 2S or 2P state may occur within the quenching cell with subsequent decay.

(iii) A large flux of H(1S) and protons enter the quenching cell and may cause excitation and/or dissociation of the residual gas with resulting photon emission.

(iv) Particle impact on surfaces may result in photons which could be registered by the photon detector.

(v) The flux of metastable particles may be low enough for dark-noise from the photon detector to be significant.

Also important are the causes of loss in the number of registered metastable particles:

(i) Decay of the metastable flux may be caused by collisions with the residual gas between the target and quenching cell.

(ii) Decay of the metastable state may be significant if large stray electric and/or magnetic fields exist between the target and quenching cell.

(iii) Incomplete decay of the metastable flux within the quenching cell must be avoided.

(iv) The placement of the photon detector and the surrounding geometry must be such as to view the complete region of the quenching cell where decay occurs.

(v) The limited solid angle of the photon detector, and the conversion efficiency of the photon detector and counting electronics must be considered.

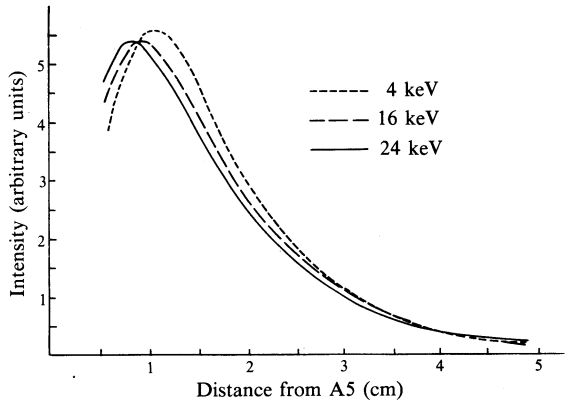

Fig. 1. Lyman α photon intensity as a function of distance of penetration of the metastable hydrogen atom into the quenching cell (see Fig. 2 in Section 6).

In any practical quenching cell there is some spatial distribution of electric field strength; therefore calculations more complex than those employing equations (2)–(4) must be performed if the lifetime, and hence the fraction quenched, is to be correctly estimated (Drake *et al.* 1975; Drake and Grimley 1973, 1975). If the fraction f of the total metastable flux which decays over the whole quenching cell is substantially less than 1, a detailed knowledge of the electric field and lifetime as a function of the field must be known in order to calculate the actual fraction quenched in the cell. Previously, short quenching fields have been used (Crandall 1970) so that at low particle velocities $f \approx 1$ but at high velocities $f < 1$. The data may be corrected using equations (2)–(4) with the assumption that the field is constant (spatially). However, such corrections must be viewed with caution because the field is generally not constant. The design of the quenching cell should ensure that under all conditions for use $f \approx 1$. Any inaccuracies in determining the electric field over the quenching

cell, in the lifetime of the particle, or in the fraction quenched are then unimportant because almost all of the metastable particles are guaranteed to have decayed.

An estimate of the overall length of the quenching cell that is required for $f \approx 1$ can be made if equations (2)–(4) are used. For 98% decay to take place, equation (4) gives a time interval greater than the lifetime of the 2S state by a factor of 4. At a beam energy of 20 keV this occurs over a distance of about 40 mm. By applying these equations the form of the intensity distribution along the axis of the quenching cell appears to be exponential. However, in practice this does not occur because the electric field is not constant. The intensity distribution of the Lyman α photons resembles that shown in Fig. 1. As the metastable atom enters and proceeds through the quenching cell it experiences an electric field that increases to an approximately constant value near the centre of the cell. The lifetime of the metastable atom decreases as it proceeds to higher electric field strengths, and the resulting photon intensity from the quenched metastable flux rises to a peak. In the region where the electric field is almost constant, the intensity distribution resembles an exponential tail.

Thus, the error in calculating the fraction quenched using equations (2)–(4) originates from the region where the atom enters the electric field. Although only a short distance is involved over which the photon intensity is integrated by the photon detector, it is in a region where the photon intensity is high. The calculated fraction quenched is therefore likely to be significantly greater than the actual fraction. To compensate for this the length of field could be arbitrarily extended to ensure that 100% decay takes place, but this is undesirable as it results in an increase in the background signal monitored by the photon detector. This background signal is directly proportional to the pathlength viewed by the photon detector. A method is discussed in Section 6 whereby the actual fraction quenched is calculated and conditions are determined to obtain $f \approx 1$ over the energy range 4–24 keV without employing a quenching cell which is oversized.

3. Anisotropy of Photon Emission

Early researchers incorrectly assumed that the electric field used to quench the 2S state would predominantly couple the $2S_{1/2}$ state to the $2P_{1/2}$ and therefore give an isotropic distribution of photon intensity. Although the Lamb shift between $2P_{1/2}$ and $2S_{1/2}$ states is only 10% of the fine structure splitting between $2P_{1/2}$ and $2P_{3/2}$ there is a significant coupling to the $2P_{3/2}$ state.

Fite *et al.* (1968), in an endeavour to explain discrepancies in the data reduction of an earlier experiment (Stebbings *et al.* 1960), conducted experiments to measure the polarisation of photon emission from the metastable state of hydrogen by quenching the 2S state in a small electric field of 15 V cm^{-1}. Using a time-independent perturbation calculation (Ott *et al.* 1970) the magnitude of the polarisation was found to be $-0{\cdot}329$. This compared reasonably well with the measured value of $-0{\cdot}30 \pm 0{\cdot}02$, although it is somewhat higher. Sellin *et al.* (1970) gave detailed calculations and measurements of the polarisation for field strengths up to 1000 V cm^{-1} where the atom enters the field over a time longer than the period associated with the fine structure splitting of the hydrogen atom (i.e. adiabatic entry conditions at $\gg 10^{-10}$ s). It was shown that the magnitude of the polarisation for larger electric field strengths approached a value of -1, and at smaller fields it is given by

$$P = (x^2 - z^2)/(x^2 + z^2), \tag{5}$$

where

$$x^2 = (6^{\frac{1}{2}}\gamma + 3^{\frac{1}{2}})^2, \tag{6}$$

$$z^2 = \{-(\tfrac{3}{2})^{\frac{1}{2}}\gamma + 3^{\frac{1}{2}}\}^2; \tag{7}$$

$$\gamma = -2^{\frac{1}{2}}(1{\cdot}058 + D)/(9{\cdot}911 - D), \tag{8}$$

where

$$D = 0{\cdot}529E/475 \tag{9}$$

is the Stark shift of the $2S_{1/2}$ level (the values of 1·058 and 9·911 GHz have been used for the zero field $2S_{1/2}$–$2P_{1/2}$ and $2S_{1/2}$–$2P_{3/2}$ splittings), and E is the magnitude of the electric field (V cm^{-1}).

When the atom enters the electric field quickly (i.e. sudden entry condition at $t \ll 10^{-10}$ s), the polarisation value approaches $+1$ (rather than -1) for increasing field strength. Crandall and Jaecks (1971) gave a detailed calculation of the time-independent magnitude of the polarisation for the sudden entry condition. Subsequently, Wooten and Macek (1972) investigated the instantaneous polarisation of the quench-induced Lyman α photons from metastable hydrogen atoms for entry conditions between the adiabatic and sudden conditions described above. The instantaneous polarisation as a function of the time after entry into the electric field was calculated and revealed oscillations when the entry time into the field was sudden ($\ll 10^{-10}$ s) or in the intermediate region ($\approx 10^{-10}$ s). Such oscillations have been observed experimentally using electric field quenching of the metastable hydrogen atom (Wijngaarden *et al.* 1976; Drake 1977).

If the polarisation of the emission can be obtained it is possible to account for the anisotropic intensity distribution of the radiation (Smit 1935):

$$I(\theta) = (I'/4\pi)(3 - 3P\cos^2\theta)/(3 - P), \tag{10}$$

where P is the magnitude of the polarisation, I' is the photon intensity integrated over all angles, θ is the angle between the direction of observation of the photon and the electric field, and $I(\theta)$ is the intensity of radiation in direction θ.

4. Accounting for Anisotropy

In the past various methods have been proposed and tested to account for the anisotropic distribution of photons resulting from the 2S–2P–1S transition:

(i) The actual polarisation may lie between the theoretical value for sudden entry and that for slow entry into the electric field. For example, at 500 V cm^{-1} the polarisation for adiabatic entry is $-0{\cdot}52$ which results in an intensity of $I(0°) = (I'/4\pi)1{\cdot}3$ or $I(90°) = (I'/4\pi)0{\cdot}85$ (from equation 10), and the polarisation for sudden entry is $-0{\cdot}2$ which results in an intensity of $I(0°) = (I'/4\pi)1{\cdot}13$ or $I(90°) = (I'/4\pi)0{\cdot}94$. The range of variation caused by the anisotropy could be incorporated into the error estimate and the recorded photon flux left unchanged (Crandall 1970).

(ii) By observing the radiation at the so-called 'magic angle', where $\cos^2\theta = \frac{1}{3}$ in equation (10), the polarisation no longer enters into this relation (see e.g. Shah *et al.* 1980).

(iii) The polarisation may be measured by using a polarisation analyser which consists of a lithium fluoride crystal set at the Brewster angle to eliminate one vibration direction (Ott *et al.* 1970). A multiple reflection analyser may also be used (Matsui and Walker 1970).

(iv) The polarisation may be measured by viewing the photon intensity in two directions, one parallel to the electric field (I'') and the other perpendicular to it (I), and using the equations (Drake *et al.* 1975)

$$R = (I''-I)/(I''+I), \qquad P = 2R/(R-1). \tag{11, 12}$$

(v) The photon detector may be calibrated with a source of radiation which has a polarisation and intensity distribution similar to the light source used in the actual measurement (Fitzwilson and Thomas 1972). For example, using a known total cross section for production of metastable hydrogen, the flux of particles decaying in view of the photon detector can be calculated and thus related to the actual number of photons measured by the detector to give its conversion efficiency. The calibrated detector may then be used for measurement of other cross sections which are unknown.

Solutions (ii)–(iv) are at the expense of the efficiency of the detector because the solid angle of the photon detector must be small to accurately account for the polarisation. A high efficiency detector is required for the measurement of differential cross sections and therefore calibration of the detector by normalisation to a total cross section from the literature appears to be the best solution. The absolute magnitude of the polarisation is not important provided the cross section to which the normalisation is made took into account polarisation. However, because the normalisation is performed at one velocity, it is important to consider the variation in efficiency of the detector at different projectile velocities. The fraction quenched depends on the time the atom spends in the field and, since a range of velocities is being considered, there results a different intensity distribution along the beam path for particle flux at different velocities. Fitzwilson and Thomas (1972) measured this variation and quoted $\pm 5\%$ over the energy range 4–20 keV. The calculated efficiency variation for the design used in this experiment is less than $\pm 2\%$ over the energy range 4–24 keV; these calculations are discussed below.

The response of the detector to each component of the polarised emission must be similar, otherwise the measurements will be characteristic of the particular detector employed (Thomas 1972). The detector used in this experiment has a small degree of 'instrumental polarisation' but this has been shown to be negligible.

5. Oscillation of the Polarisation

Theory (Wooten and Macek 1972; Drake *et al.* 1975; Drake and Grimley 1975) and experiment (Drake 1977) revealed damped oscillations in the magnitude of the polarisation of the photon emission from H(2S) lasting up to 30 ns from the time that the field is applied to the metastable atom. These oscillations cause a spatial

modulation in the emission intensity into a particular direction, although the intensity integrated over all angles does not oscillate. Wooten and Macek (1972) gave the criterion which must be fulfilled if oscillations are to be avoided. The metastable atom must be subjected to the field over a time much greater than 10^{-10} s (adiabatic entry condition). It should be noted that it is the time over which the action is applied that is of main importance rather than the magnitude or rate of change of the electric field with distance. Once the oscillations start they last for a substantial period of time. Their calculations showed that small amplitude oscillations are produced for a 0·4 ns perturbation, but no oscillations occur for a 1·2 ns perturbation. For small amplitude oscillations the polarisation integrated over distance into one direction is almost the same as the polarisation without oscillation, but as the perturbation time decreases the oscillations grow in amplitude and the integrated polarisation departs from the adiabatic value. These oscillations are undesirable as their spatial period is directly related to the particle velocity and therefore could produce changes in the detector's conversion efficiency.

The perturbation is produced around the aperture which separates the field-free region between the target and this aperture from the electric field within the quenching cell. The perturbation in the electric field is related to the size of the aperture separating these regions. This aperture is primarily used to define the solid angle of the scattered flux and was in our case approximately 0·35 mm wide. If it were used to perform this partitioning function between the electric field and field-free region, the perturbation could be as quick as $\approx 10^{-10}$ s. However, to avoid the oscillation, another aperture was introduced after the one which defined the solid angle of the scattered flux. Its size and separation from the first aperture were adjusted to give a perturbation caused by the electric field over a sufficiently long time so that oscillations were unlikely to occur.

Calculation of the magnitude and direction of the electric field around a circular aperture has been given by Drake (1977) and reveals a rise from zero to a steady field over a distance either side of the aperture of approximately one quarter of its diameter. Also, the field direction as experienced by the atom rotates on passing through the aperture; therefore the emission intensity in the direction of the photon detector can change. The effect of this field rotation, however, is small since the magnitude of the field around this position is such that the quenching in this region is an insignificant contribution to that from the whole quenching cell. The diameter selected to ensure adiabatic entry into the quenching field and so ensure small (0·5–2%) prequench loss due to unobserved quenched flux is 5·5 mm. This gives a perturbation distance of approximately 2·8 mm which corresponds to a 3·2 ns perturbation at 4 keV and 1·3 ns at 24 keV. Therefore no oscillations should occur.

6. Design and Testing of the Detector

The important dimension of the quenching cell is its length. A calculation was performed to find the length over which a field must act so that, at the greatest particle velocity and at the minimum lifetime of the particle, the fraction quenched is more than 98%. The variation in the efficiency of the conversion process over the whole energy range of the experiment was also considered. The calculation was performed for a beam travelling along the axis of the quenching cell by dividing the total length of the cell into 50 equal parts. The equation for the total fraction

quenched is a variation of equation (4), namely

$$f = \sum_{i=0}^{N} F_i, \tag{13}$$

where

$$F_i = \left(1 - \sum_{j=0}^{i-1} F_j\right)[1 - \exp\{-\mathrm{i}\, L_{56}/N v t(2\mathrm{S})_i\}] \tag{14}$$

is the fraction quenched in segment i ($F_0 = 0$), N is the number of segments ($=50$), L_{56} is the length of the quenching cell, v is the beam velocity, $t(2\mathrm{S})_i$ is the lifetime of the metastable atom calculated using equations (2) and (3) and the average electric field within the segment i. This average field $E(z)$ along the axis of the quenching cell was calculated using the equation given by Wijngaarden and Drake (1978):

$$E(z) = E(\tfrac{1}{2}L_{56})\, 2\sin(z\pi/L_{56})/\{1 + \sin^2(z\pi/L_{56})\}, \tag{15}$$

where $E(\frac{1}{2}L_{56})$ is the electric field at the centre of the quenching cell, and z is the distance along the axis of the cell (centre $= \frac{1}{2}L_{56}$).

To account for variation in detection efficiency along the pathlength of the beam, the photon flux from each segment S_i which reaches the photon detector was calculated by multiplying the fraction quenched F_i from a segment i (equations 13 and 14) by the solid angle of the photon detector Ω_i, and the intensity in the direction of the photocathode adjusted for polarisation and anisotropy of the emission A_i:

$$S_i = F_i\, \Omega_i\, A_i, \tag{16}$$

where

$$\Omega_i = \pi R_\mathrm{p}^2\, L/[L^2 + \{(i - \tfrac{1}{2}N)L_{56}/N\}^2]^{\frac{3}{2}}, \tag{17}$$

$$A_i = 3(1 - P_i \cos^2 \alpha_i)/(3 - P_i); \tag{18}$$

$$\alpha_i = \tan^{-1}[\{(i - \tfrac{1}{2}N)^2\}^{\frac{1}{2}} L_{56}/LN] \quad \text{or} \quad \tfrac{1}{2}\pi. \tag{19, 20}$$

Here R_p is the radius of the cathode of the photon detector, L is the distance from the cathode of the photon detector to the beam axis, and P_i is the polarisation at segment i calculated from equations (5)–(9) for the electric field calculated from equation (15). Equation (19) or (20) is substituted into (18). Equation (19) applies when the direction of the electric field and the direction of the axis of the photon detector are parallel; equation (20) applies when the directions of the electric field, metastable flux and axis of the photon detector are orthogonal.

The total intensity reaching the detector S is the photon flux from each segment S_i summed over all segments:

$$S = \sum_{i=0}^{N} S_i. \tag{21}$$

The fraction quenched f and the photon intensity S were calculated for various cell lengths, applied potentials, and beam velocities. The variations in intensity along the quenching cell with beam velocity are shown in Fig. 1 (Section 2).

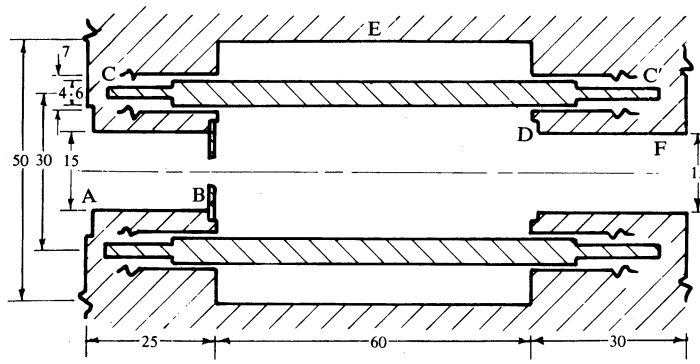

Fig. 2. Dimensions of the quenching cell which characterise the electric field. The labels refer to the following: A, recess for disc with aperture A4 (aperture normally installed); B, disc (19 mm) with aperture A5; C and C′, mounting of quench rods not shown; D, recess for disc with aperture A6 (disc not normally installed); E, aperture window to the photomultiplier tube (not shown in this cross section), dimensions are 5×48 mm starting from the A5 plane; F, position of secondary emission detector (not shown).

Table 1. Variation in detection efficiency (relative to the absolute efficiency of the detector at 16 keV) for various proton energies and for electric field directions both parallel and perpendicular to the axis of the photon detector

Beam energy (keV)	Electric field[A] (V cm^{-1})	Efficiency variation (%) 0°	90°	Response rate ratio[B]
4	228	−2·4	+1·8	1·39
8	303	−1·5	+1·1	2·42
16	435	0	0	1·46
24	580	+1·6	−1·2	1·50

[A] At centre of cell for a fraction of 99%. [B] Rate of response at 0° to that at 90°.

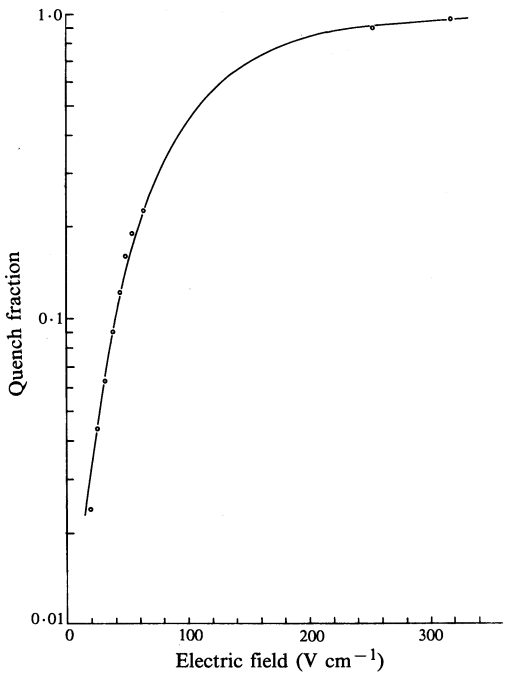

Fig. 3. Quench factor against electric field at centre of quench cell. Circles represent measured quench fractions at a beam energy of 16 keV for a quench cell length of 60 mm while viewing photons in the direction of the applied field. The curve shows corresponding theoretical data.

The lifetime of the 2S state for large fields (>600 V cm^{-1}) is almost constant, approaching twice that of the field-free lifetime of the 2P state; this limits the smallest length of quenching cell that can be used for the maximum velocity required. For cell lengths around 40–50 mm and $E(\frac{1}{2}L_{56}) = 650$ V cm^{-1} the fraction quenched at 24 keV is 96–98% respectively, and the overall efficiency at 24 keV (relative to 4 keV) decreases by 7–5% respectively. Hence a more desirable situation occurs with increasing cell lengths. The variation in efficiency over the velocity range becomes less and the fraction quenched approaches 100% for field strengths lower than the saturation value. A cell length of 60 mm (Fig. 2) was chosen because this gave an efficiency variation with velocity that was acceptable and saturation was assured even if the data used in the calculations outlined above were in some error. The efficiency variation for different velocities and for a cell length of 60 mm is given in Table 1.

The constant of proportionality between the potential applied to the electrodes of the quenching field ξ and the magnitude of the electric field at the centre of the cell has been calculated by Drake (1977):

$$E(\tfrac{1}{2}L_{56}) = \pm 0{\cdot}544\xi\,. \tag{22}$$

However, this calculation was based on electrode dimensions and boundary conditions that were different to those employed in the present experiment (see Fig. 2) and may therefore not be applicable in our case. It is desirable to 'measure' the constant of proportionality between the applied potential and the resulting electric field at the centre of the cell.

A calculation may be used to obtain a plot of the fraction quenched against the electric field at the centre of the cell. The results show a linear increase in fraction quenched at small fields, whereas at high fields the gradient of the curve approaches zero (saturation). Measurements of fraction quenched against the potential applied to the quench electrodes show a similar dependence, namely a linear and a saturation region. By comparing the gradients of the two curves in the linear region a constant of proportionality can be obtained which relates the applied potential to the electric field (at the centre of the cell) used in the theoretical calculation. It was found that, by multiplying this constant by the applied potential, the curves of fraction quenched against applied potential and against electric field match well in the range 20–340 V cm^{-1} (see Fig. 3). The multiplication factor obtained by this method is $0{\cdot}635 \pm 6\%$, that is $E(\frac{1}{2}L_{56}) = \pm 0{\cdot}635\xi$.

Thus, the potential applied to the quench electrodes could be set to give electric field magnitudes at the centre of the cell such that the fraction quenched would remain constant at different beam velocities; this reduces the amount of variations of efficiency of the detector with velocity. After calculating the electric field required at various proton energies Φ it became obvious that the electric field could be linearly related to the particular beam velocities employed by using the approximate expression

$$\pm\xi = 254 + \tfrac{1}{36{\cdot}8}\Phi, \tag{23}$$

where ξ is in V with one pair of electrodes at $+\xi$ and the other pair at $-\xi$, and Φ is in eV.

7. Calibration

A photomultiplier tube was selected (EMI G26L315A with MgF_2 window) which provides high efficiency that peaks close to 121·6 nm. Many of the problems associated with the calibration of the Lyman α photon detector may be overcome by measuring relative cross sections and standardising these results to some reliable absolute cross section. While absolute calibrations of photometric systems can be performed without optical standards (Cristofori *et al.* 1963; Sheridan 1969), the procedure we have adopted is commonly employed, and absolute measurements (see e.g. Andreev *et al.* 1966, 1967; Suchannek and Sheridan 1975; Shah *et al.* 1980) are more the exception. In our experiment, calibration of the detector has been performed for the reaction given by equation (1) at 16 keV. The value of the total cross section reported by Shah *et al.* (1980), $2{\cdot}56\times10^{-17}$ cm^2, for the process has been employed for the normalisation of our total and differential cross sections.

The total cross sections reported here have been performed over collection angles of ±27′ and ±51′ at 8, 16, 20 and 24 keV. It would be expected that if the collection angles were too small the resulting measured total cross sections would be small. However, the results obtained with the ±27′ collection angle are not significantly different to those taken at ±51′ (within the statistical uncertainty). It may be concluded that, for the H_2 target, major scattering occurs at angles less than 27′.

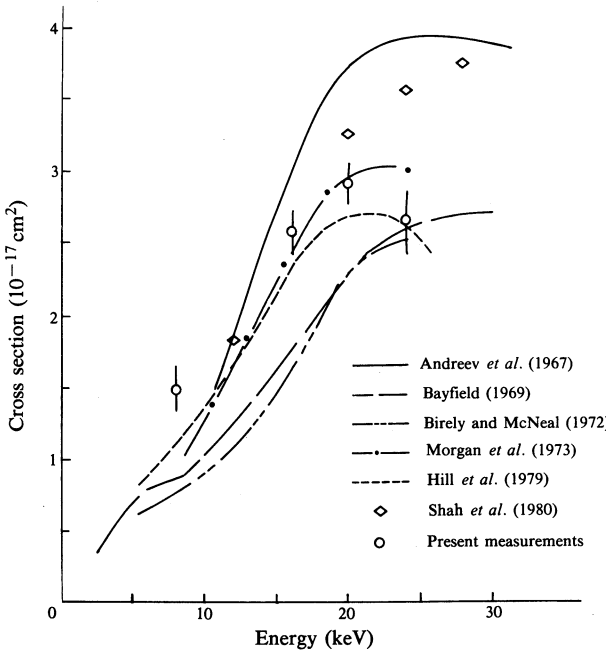

Fig. 4. Total cross sections measured as a function of energy for the electron capture reaction $H^+ + H_2 \rightarrow H(2S) + H_2^+$.

Relative total cross sections were obtained by measuring the scattered flux for several (5–9) target gas pressures. A linear regression analysis was used to determine the total cross section from the gradient of the curve of pressure (x-axis) to the ratio of scattered flux to incident flux (y-axis). The relative total cross section was then assigned the absolute value measured by Shah *et al.* (1980). The error in cross section was determined from the standard deviation of the gradient. No trend from linearity

either due to secondary collisions or due to the change in background gas pressure was found. Deviations of data from the curve of best fit were generally only a few per cent and represent a combined random error resulting from the finite count of signal and background, from fluctuations in, and measurements of, the projectile flux, and from the pressure measurement.

Fig. 4 displays the total cross sections for $H^+ + H_2 \rightarrow H(2S)$ measured as a function of energy, from the present work and previous authors. The results of Andreev *et al.* (1967) and Shah *et al.* (1980) are absolute measurements since the absolute efficiency of their photon detector was obtained from another experiment. Their detector was a photo-ionisation device which produces a current when Lyman α photons pass through a chamber filled with nitric oxide. The absolute photo-ionisation yield for nitric oxide at 121·6 nm was taken to be that reported by Watanabe *et al.* (1967). The remaining data in Fig. 4 are from experiments that employed photomultipliers that are calibrated, or the cross section results normalised, by reference to previously measured total cross sections at a single energy.

As can be seen from Fig. 4, the data available from the various laboratories for the total cross section for capture into the 2S state of hydrogen are scattered and vary in absolute magnitude, rate of rise with respect to energy, and peak position of the total cross section. Perhaps coincidentally, those cross section measurements which employed the nitric oxide photo-ionisation detector (Andreev *et al.* 1967; Shah *et al.* 1980) exhibit a steeper gradient with respect to energy than those employing a photomultiplier tube without any special filtering (Bayfield 1969; Hill *et al.* 1979; present results). It is known that the photo-ionisation yield for nitric oxide has a minimum at 121·6 nm and rises 16% to a peak at 121·2 nm and rises 24% to a peak at 122·3 nm (Nicholson 1963; Fig. 4 therein). It may well be that the efficiency of the nitric oxide photo-ionisation detector increases sufficiently with projectile energy, due to Doppler shifted Lyman α photons, to cause a part of the observed difference between laboratories. The total cross section for $H^+ + Ar \rightarrow H(2S)$ has been reported by Shah *et al.* (1980; Fig. 6 therein) and a summary of previous work given. A comparison of these cross sections also demonstrates two gradients depending on the type of photon detection employed.

Other possible causes for the difference in gradient that have been considered, by a comparison of the experimental arrangement of the various workers, are:

(i) That a change of collection efficiency of the photon detector is caused by the anisotropic distribution of the quenched metastable particles. The gradient obtained in the present results is different to that reported by Shah *et al.* (1980), yet in both arrangements the anisotropic distribution was taken into account so that the detection efficiency would not vary greatly. Also, the gradients of the data for Andreev *et al.* (1967), Birely and McNeal (1972) and Morgan *et al.* (1973) are similar to that of Shah *et al.* (1980); however, the results by Shah *et al.* (1980) should be more reliable than these because the polarisation was considered.

(ii) A different rate of population of the metastable state from higher states (cascade) may occur due to the application of an electric field in the target region (Andreev *et al.* 1967; Birely and McNeal 1972; Morgan *et al.* 1973) or due to the different decay pathlengths of the higher states (Shah *et al.* 1980, 10 cm; Bayfield 1969, 260 cm; present results, 32 cm). However, the difference in the gradients is not consistent with this cause.

(iii) For those groups that viewed the target region (Andreev *et al.* 1967; Birely and McNeal 1972; Morgan *et al.* 1973), the Lyman α photons produced from dissociative excitation of the H_2 target are unlikely to cause the problem because these results are consistent with those reported by Shah *et al.* (1980) where a 10 cm pathlength was employed between the target and detector.

(iv) The angular range accepted by the detector, used to define the total cross section, does not seem to be the cause (Shah *et al.* 1980, 36′ minimum; Bayfield 1969, 11′ maximum; present results 27′ and 51′ minimum).

(v) Collisional loss in all the experiments was negligible and is unlikely to be a cause.

The question as to the reason for the two different gradients of the total cross section against energy is an important one to examine, considering the usefulness of the results such as those reported by Shah *et al.* (1980) for normalisation of other cross sections. The change in efficiency of the nitric oxide photo-ionisation detector over a small wavelength interval certainly makes the question worthy of further consideration in future, perhaps by employing both a photo-ionisation detector and a photomultiplier and comparing their relative efficiencies with respect to metastable particle energy.

Comparisons of the present total cross sections at 16 keV with other gases (helium and argon) are consistent with, although less accurate than, those reported by Shah *et al.* (1980). For helium, Shah *et al.* reported $0{\cdot}156\pm0{\cdot}006$(one standard deviation)$\times10^{-17}$ cm^2, while the present measurement is $0{\cdot}174\pm0{\cdot}028$(one standard deviation)$\times10^{-17}$ cm^2. For argon, Shah *et al.* reported $(3{\cdot}10\pm0{\cdot}012)\times10^{-17}$ cm^2, while the present measurement is $(3{\cdot}23\pm0{\cdot}35)\times10^{-17}$ cm^2.

Acknowledgment

One of us (D.G.W.) acknowledges the receipt of a La Trobe University Postgraduate Scholarship.

References

Andreev, E. P., Ankudinov, V. A., and Bobashev, S. V. (1966). *Sov. Phys. JETP* **23**, 375–82.
Andreev, E. P., Ankudinov, V. A., Bobashev, S. V., and Matveyer, V. (1967). *Sov. Phys. JETP* **25**, 232–5.
Bayfield, J. E. (1969). *Phys. Rev.* **182**, 115–28.
Bethe, H. A., and Salpeter, E. E. (1957). *In* 'Encyclopedia of Physics', Vol. XXXV, Sections 63 and 67 (Springer: Berlin).
Birely, J. H., and McNeal, R. J. (1972). *Phys. Rev.* A **5**, 692–701.
Brouillard, F. (1981). *Phys. Scr.* **23**, 163–9.
Crandall, D. H. (1970). Ph.D. Thesis, University of Nebraska.
Crandall, D. H., and Jaecks, D. H. (1971). *Phys. Rev.* A **4**, 2271–80.
Cristofori, F., Fenici, G. E., Molho, N., and Sona, P. G. (1963). *Phys. Lett.* **6**, 171.
Drake, G. W. F. (1977). *J. Phys.* B **10**, 775–82.
Drake, G. W. F., Farago, P. S., and Van Wijngaarden, A. (1975). *Phys. Rev.* A **11**, 1621–8.
Drake, G. W. F., and Grimley, R. B. (1973). *Phys. Rev.* A **8**, 157–60.
Drake, G. W. F., and Grimley, R. B. (1975). *Phys. Rev.* A **11**, 1614–20.
Fite, W. L., Kauppila, W. E., and Ott, W. R. (1968). *Phys. Rev. Lett.* **20**, 409–10.
Fitzwilson, R. L., and Thomas, E. W. (1972). *Phys. Rev.* A **6**, 1054–63.
Homma, H., Lewis, R. R., and Robiscoe, R. T. (1982). *Phys. Rev.* A **25**, 333–6.
Hill, J., Geddes, J., and Gilbody, H. B. (1979). *J. Phys.* B **12**, L341–4.

Matsui, A., and Walker, W. C. (1970). *J. Opt. Soc. Am.* **60**, 64–5.
Morgan, T. J., Geddes, J., and Gilbody, H. B. (1973). *J. Phys.* B **6**, 2118–38.
Nicholson, A. J. C. (1963). *J. Chem. Phys.* **39**, 954–61.
Ott, W. R., Kauppila, W. E., and Fite, W. L. (1970). *Phys. Rev.* A **1**, 1089–98.
Sellin, I. A. (1964). *Phys. Rev.* **136**, A 1245–53.
Sellin, I. A., Biggerstaff, J. A., and Griffin, P. M. (1970). *Phys. Rev.* A **2**, 423–9.
Shah, M. B., Geddes, J., and Gilbody, H. B. (1980). *J. Phys.* B **13**, 4049–58.
Sheridan, J. R. (1969). *Rev. Scient. Instrum.* **40**, 358–9.
Smit, J. A. (1935). *Physica* **2**, 104–10.
Stebbings, R. F., Fite, W. L., Hummer, D. G., and Brackman, R. T. (1960). *Phys. Rev.* **124**, 2051(E).
Suchannek, R. G., and Sheridan, R. J. (1975). *Phys. Rev.* A **12**, 460–7.
Thomas, E. W. (1972). 'Excitation in Heavy Particle Collisions' (Wiley: New York).
Watanabe, K., Matsunaga, F. M., and Sakai, H. (1967). *Appl. Opt.* **6**, 391–6.
Wijngaarden, A., and Drake, G. W. F. (1978). *Phys. Rev.* A **17**, 1366–74.
Wijngaarden, A., Goh, E., Drake, G. W. F., and Farago, P. S. (1976). *J. Phys.* B **9**, 2017–25.
Wooten, J. W., and Macek, J. H. (1972). *Phys. Rev.* A **5**, 137–40.

Manuscript received 2 April, accepted 1 August 1986